ELSEVIER

Materials Science and Engineering A 449–451 (2007) 649–653

MATERIALS SCIENCE & ENGINEERING A

www.elsevier.com/locate/msea

Dendritic solidification and fragmentation in undercooled Ni–Zr alloys

P.K. Galenko *, G. Phanikumar, O. Funke, L. Chernova, S. Reutzel, M. Kolbe, D.M. Herlach

German Aerospace Center (DLR), Institute of Space Simulation, 51170 Cologne, Germany

Received 21 August 2005; received in revised form 28 October 2005; accepted 24 February 2006

Abstract

Kinetics of dendritic solidification and fragmentation of dendritic crystals in undercooled Ni–Zr samples are studied. Using the capacitance proximity sensor technique and a high-speed-camera system, the dendrite growth velocity has been measured as a function of initial undercooling in solidifying droplets processed by the electromagnetic levitation technique. Analyses of solidified droplets give evidence to a transition from coarse grained dendrites to grain refined dendrites (CG-GR) at small undercooling, a transition from grain refined dendrites to coarse grained dendrites (GR-CG) at moderate undercooling, and to a second transition from coarse grained dendrites to grain refined dendrites (CG-GR) at a higher undercooling. Predictions of a sharp-interface model are compared with the results of experiments on Ni–Zr samples.

Keywords: Dendrite; Solidification; Diffusion; Undercooling; Alloy; Model

1. Introduction

Solidification of undercooled Ni–Zr alloys has been investigated recently [1,2] at small concentrations of Zr. Dendritic growth velocities V have been measured in Ref. [1] as a function of undercooling ΔT in levitated droplets of $Ni_{99}Zr_1$ (numbers indicate at.%) alloys using electromagnetic levitation technique (see overview [3]). The results have been described within the LKT/BCT model of dendrite growth [4,5]. With increase of the undercooling, solute trapping becomes important in rapid solidification which leads to deviation from local chemical equilibrium at the solid–liquid interface. In the LKT/BCT model of dendrite growth [4,5], this phenomenon is introduced by the solute partitioning function $k(V)$ which adopts interfacial diffusion speed V_{DI} as a kinetic parameter of solidification [6]. The diffusion speed V_{DI} has been independently determined by pulsed laser experiments [1] on thin specimens for the $Ni_{99}Zr_1$ alloy. Together with preliminary used parameters of Ni–Zr alloys, the measured results for V_{DI} encouraged the prospects of a parameter-free test of the LKT/BCT model. In addition, the dendritic structure of solidified droplets from $Ni_{99.5}Zr_{0.5}$ and $Ni_{99}Zr_1$ alloys has been evaluated [2] to find morphological transitions in dendritic pattern. The results of metallographic analysis were compared with the predictions of Karma's model [7,8] of grain refinement *via* dendritic fragmentation.

Further progress on experimental measurements and theoretical description of dendritic growth and fragmentation in Ni–Zr alloys is presented in this paper. First, the photo-diode technique as used in Refs. [1,2] is improved by application of capacity proximity sensor (CPS) and by a high-speed camera (HSC) to measure dendritic growth velocity in levitated droplets. Second, the dendrite growth kinetics is tested experimentally to verify the idea that small amounts of impurity may enhance the solidification velocity of diluted alloys in comparison with the solidification velocity of pure systems. Third, the predictions of a model for rapid dendritic growth [9], which assumes deviation from local equilibrium at the interface and in the solute diffusion field are compared with the experimental dendrite velocities in Ni–Zr alloys. Fourth, metallographic analysis of solidified samples is made to measure the size of the dendritic structure and to evaluate critical undercoolings for dendritic fragmentation and coarsening. These findings for various Ni–Zr alloys extend previous investigations [1,2] on kinetics of solidification and fragmentation of dendritic crystals.

2. Experimental details

An electromagnetic levitation facility was used to undercool the samples and to measure the velocity of solidification, the standard setup is described elsewhere [10,11]. In contrast to the

* Corresponding author. Fax: +49 2203 6012255.
E-mail address: peter.galenko@dlr.de (P.K. Galenko).

0921-5093/$ – see front matter © 2006 Elsevier B.V. All rights reserved.
doi:10.1016/j.msea.2006.02.435

photo-diode technique [1,2], the present CPS technique uses two separate signals and the velocity of solidification is measured over the complete sample diameter. First signal: the change of capacitance of an oscillating circuit, which is caused by touching the levitated sample at the south pole with a trigger needle; second signal: the change of brightness caused by the release of latent heat at the north pole of the sample at the end of the solidification process, which is detected by a photodiode.

The HSC measurement allows for detecting the morphology of the solidification front at a frequency up to 120,000 Hz depending on the resolution. This enables us to detect small deviations of the growth direction from the vertical line caused by minor deviations of the trigger point from the south pole of the levitating and oscillating specimen. Parameters for the evaluation of the growth velocity, solidification length h and solidification time Δt, are defined with a smaller error, and hence HSC technique is the most accurate technique for detecting growth velocities from the undercooled melts at elevated temperatures.

$Ni_{99.9}Zr_{0.1}$, $Ni_{99.5}Zr_{0.5}$ and $Ni_{99}Zr_1$ alloys of about 1.0 g of mass were prepared from constituents of Ni and Zr both of 99.99% purity. These diluted Ni–Zr alloys were chosen for investigation due to their undercoolability in electromagnetic levitation experiments, and availability of their thermodynamic and kinetic data [1,2]. Moreover, strong chemical inhomogeneity existing during solidification of these alloys (due to small value of equilibrium partition coefficient of Zr in Ni) may lead to two interesting effects. First, it may exhibit the enhancement of dendrite growth for very small controlled amounts of Zr in Ni. And, second, it may exhibit a strong solute trapping giving evidence of the transition from solute diffusion-limited growth to thermally controlled growth of dendrites.

3. Experimental results

3.1. Growth

The new results found by CPS and by HSC confirm the correctness of the previous data [2] using photo-diode technique. They have lower experimental scatter due to methodical and technical improvements of the measurements. The small controlled amounts of Zr in Ni give enhancement of the growth velocity for solidifying $Ni_{99.9}Zr_{0.1}$ alloys in comparison with the "nominally pure" nickel. This finding confirms previous outcome [13,14] that a low amount of impurity in a pure system may enhance the growth velocity of dendritic crystals in the range of small or even moderate undercoolings. The experiments with $Ni_{99.5}Zr_{0.5}$ and $Ni_{99}Zr_1$ confirm a well established fact that the dendrite growth velocity V decreases at a given undercooling ΔT with increasing concentration of impurity [15].

3.2. Fragmentation

The microstructure of $Ni_{99}Zr_1$ has been analyzed metallographically after solidification. The following sequence of microstructures has been found: coarse grained (CG) microstructure at $\Delta T = 37$ K; transition region of undercoolings 37 K $< \Delta T <$ 80 K; grain refined (GR) microstructure in the region 80 K $< \Delta T <$ 123 K; transition region of undercoolings 123 K $< \Delta T <$ 130 K; coarse grained (CG) dendritic microstructure in the region 130 K $< \Delta T <$ 177 K. In the indicated transition regions of undercoolings, both microstructures (CG and GR) were found. These regions of uncertainty can be explained by influence of forced convective flow during solidification of levitated droplets [12].

The microstructures are shown in Fig. 1. Fig. 2 (top figure) demonstrates the experimental size of dendrites versus undercooling in the droplet for the present results. For completeness the previous results from [2] have been drawn to Fig. 2. Pre-

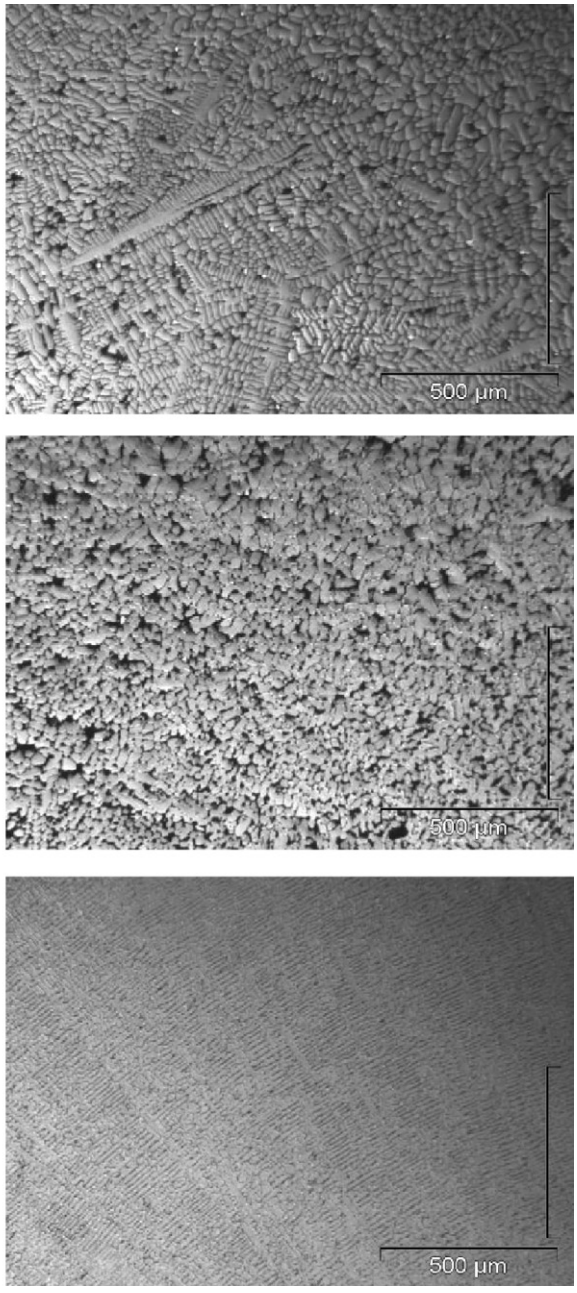

Fig. 1. Microstructure in $Ni_{99}Zr_1$ alloy. (a) CG (Coarse-Grained) dendritic pattern: $\Delta T = 37$ K; (b) GR (grain-refined) dendritic pattern: $\Delta T = 80$ K; (c) CG (coarse-grained) dendritic pattern: $\Delta T = 155$ K.

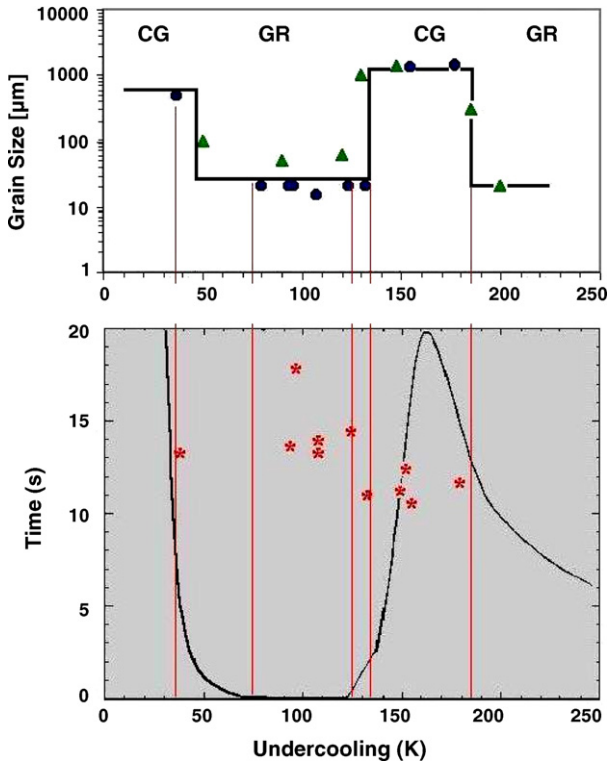

Fig. 2. Top: measured dendritic grain size for given sample (i.e. for given undercooling) of $Ni_{99}Zr_1$ alloy. Triangles were taken from [2], filled circle are the results of the present investigation. Bottom: computed time for break-up (8) of dendritic structure (solid line) and experimental plateau time (stars).

viously, only the transitions GR → CG → GR were found in Ni–Zr alloys [2]. In addition, we found the transition CG → GR at small undercoolings. Thus, the complete sequence of dendritic microstructure is given by CG → GR → CG → GR.

4. Sharp-interface model

Due to the fact that experimental data on solidification of the Ni–Zr alloys cover a wide range of undercoolings up to 288 K and dendrite growth velocity up to 30 m/s, we have chosen the sharp-interface model of dendritic growth [9]. The sharp-interface model provides the ability to describe diffusion-limited growth of dendrites (growth of "solutal" dendrites at low undercoolings), both diffusion-limited and thermally controlled growth of dendrites (growth of "solutal" and "thermal" dendrites in the intermediate range of undercoolings), and purely thermally controlled dendritic solidification at higher undercoolings. The description of dendritic growth in the whole range of undercooling is possible by introducing both deviations from local equilibrium at the interface and in the solute diffusion field, which both play an important role at high solidification velocity.

The dendrite tip radius R and the dendrite tip velocity V as the main characteristics of primary dendrites are obtained from the steady-state model of an axis-symmetric dendritic growth in an undercooled binary system [9]. The final governing equations are summarized as follows. For the total undercooling $\Delta T = T_M + mC_0 - T_0$ the final balance at the dendrite tip is given by:

$$\Delta T = \Delta T_T + \Delta T_C + \Delta T_N + \Delta T_R + \Delta T_K, \tag{1}$$

where C_0 and T_0 are the initial composition and temperature, respectively, $\Delta T_T = (Q/c_p)Iv(P_T)$ the thermal undercooling, $\Delta T_N = (m - m_v)C_0$ the undercooling arising due to the shift of equilibrium liquidus from its equilibrium position in the kinetic phase diagram of steady-state solidification, $\Delta T_R = 2d_0Q/(c_pR)$ the curvature undercooling due to the Gibbs-Thomson effect, and $\Delta T_K = V/\mu_k$ the kinetic undercooling. The notations for material parameters presented below are given in Ref. [12]. Note that if the dendrite tip velocity V is equal to or greater than the solute diffusion speed V_D the constitutional undercooling ΔT_C is equal to zero exactly

$$\begin{aligned} &\Delta T_C = k_v\Delta_v\frac{Iv(P_C)}{1-(1-k_v)Iv(P_C)}, \quad \text{with } V < V_D,\\ &\Delta T_C = 0, \quad \text{with } V \geq V_D \end{aligned} \tag{2}$$

In the above expressions, the Ivantsov function is given by $Iv(P) = P\exp(P)\int_P^\infty \exp(-x)/x\mathrm{d}x$ with the thermal Peclet number $P_T = VR/2a$ and solutal Peclet number $P_C = VR/2D$. The velocity dependent non-equilibrium interval Δ_v of solidification in Eq. (2) is described by:

$$\begin{aligned} &\Delta_v = \frac{m_vC_0(k_v-1)}{k_v}, \quad \text{with } V < V_D,\\ &\Delta_v = 0, \quad \text{with } V \geq V_D. \end{aligned} \tag{3}$$

In Eqs. (2) and (3), the non-equilibrium solute partitioning function k_v is given by [16]:

$$\begin{aligned} &k_v(V) = \frac{(1-V^2/V_D^2)k_e + V/V_{DI}}{(1-V^2/V_D^2)[1-(1-k_e)C_L^*] + V/V_{DI}} \quad \text{with } V < V_D,\\ &k_v(V) = 1 \quad \text{with } V \geq V_D. \end{aligned} \tag{4}$$

with the liquid concentration C_L^* at the tip of a paraboloid of revolution [17]:

$$\begin{aligned} &C_L^* = \frac{C_0}{1-(1-k_v)Iv(P_C)}, \quad \text{with } V < V_D.\\ &C_L^* = C_0, \quad \text{with } V \geq V_D. \end{aligned} \tag{5}$$

The slope m_v of the liquidus line in the kinetic phase diagram is described by [18]:

$$\begin{aligned} &m_v(V) = \frac{m_e}{1-k_e}\left\{1-k_v\left[1-\ln\left(\frac{k_v}{k_e}\right)\right] + (1-k_v)\left[\ln\left(\frac{k_v}{k_e}\right) + (1-k_v)\frac{V}{V_D}\right]\right\} \quad \text{with } V < V_D,\\ &m_v(V) = \frac{m_e\ln k_e}{1-k_e} \equiv \text{const}, \quad \text{with } V \geq V_D. \end{aligned} \tag{6}$$

The condition (2) of the absence of constitutional undercooling at $V \geq V_D$ follows from the analytical solution of the model of solute diffusion applicable for rapid solidification [19]. In such a case, the liquidus and solidus lines are merging into one line in the kinetic phase diagram of the alloy, and the non-equilibrium interval of solidification becomes zero exactly, Eq. (3). Therefore, the critical point $V = V_D$ is considered as a finite velocity, at which complete solute trapping $k_v = 1$ occurs, Eq. (4), and solidification proceeds with the initial (nominal) composition C_0, Eq. (5). At this point, $V = V_D$, a transition from the solutal and thermal dendrites is ending with the onset of the diffusionless solidification and the beginning of the purely thermal growth of dendrites.

The balance of undercoolings (1) represents the only equation for two variables, namely, the dendrite tip velocity V and dendrite tip radius R. The second equation for these two variables can be obtained from the stability analysis for selection of the stable mode of the dendritic tip. This analysis gives the following expressions:

$$\frac{2d_0a}{VR^2} = \sigma_0\varepsilon^{7/4}\left[\frac{1}{2}\xi_T(P_T) + \frac{ac_p}{DQ}\frac{\Delta_v k_v}{[1-(1-k)Iv(P_C)]}\xi_C P_C\right], \quad \text{with } V < V_D, \tag{7}$$

$$\frac{2d_0a}{VR^2} = \frac{\sigma_0\varepsilon^{7/4}}{2}\xi_T(P_T), \quad \text{with } V \geq V_D.$$

where ξ are the stability functions dependent on thermal Peclet numbers P_T and P_C, and ε the strength of anisotropy of the surface tension at the solid–liquid interface. For the conditions of relatively small growth velocity, $V \ll V_D$, the following expressions for the stability functions ξ were found [20,21]: $\xi_T(P_T) = (1 + a_1 P_T^2\varepsilon)^{-1}$ and $\xi_C(P_C) = 2(1 + a_2 P_C^2\varepsilon)^{-1}$. These are true for arbitrary Peclet numbers, existence of anisotropy of surface tension, and with neglecting the atomic kinetics on the interface. In these expressions, the numeric coefficients, $\sigma_0 = 1/0.42$, $a_1 = 0.3$, $a_2 = 0.6$ can be taken in agreement with the asymptotic analysis [22]. Assuming these functions for rapid dendritic growth, one may take Eq. (7) as second equation in addition to Eq. (1) to obtain velocity V and radius R for the dendritic tip.

5. Discussion

5.1. Growth

The predictions of the model (1)–(7) in comparison with experimental data found for solidification of a "nominally pure" Ni [13,14] and present results for the $Ni_{99.9}Zr_{0.1}$ and $Ni_{99}Zr_1$ alloys are shown in Fig. 3. Material parameters of the alloys are given in Tables of Ref. [12]. It can be seen that the dendritic growth in Ni-0.1 at.% Zr exhibits enhancement of the velocity at small undercooling (up to 80 K) in comparison with the growth of "nominally pure" nickel (concentration of impurities are on the level of 0.01 at.%). At higher undercooling, consistent with $V = V_D$, the model predicts a change of growth mechanism which gets pronounced the more Zr is included. The calculated curve of $Ni_{99}Zr_1$ exhibits this change, which can be explained by the ending of the transition from solutal and thermal dendrites to thermal dendrites [9]. It leads to diffusionless dendritic growth with sharp change in the relationship "dendrite tip radius R – undercooling ΔT". Due to the limited number of data points at undercoolings $\Delta T > \Delta T(V_D)$, the predicted general change of growth mechanism is not apparent considering the current experimental data but is clearly indicated by the experiments of Schwarz et al. [1,2].

Computed curves R–ΔT for $Ni_{99.9}Zr_{0.1}$ and $Ni_{99}Zr_1$ are shown in Fig. 4 in comparison with one for the "nominally pure" Ni. It can be seen that with the increase of concentration (from 0.1 at.% to 1.0 at.% of Zr) the onset of diffusionless solidification leads to a stronger change in dendrite tip radius at $R[\Delta T(V_D)]$.

5.2. Fragmentation

From the model of Karma [7,8] follows that the dendrite break-up during recalescence requires a characteristic duration in time, $\Delta t_{bu}(\Delta T)$, which depends on the undercooling. Let Δt_{pl} be the plateau duration found from the experimental "temperature–time" curves of a processed sample. The transition CG ↔ GR between two microstructures takes place, if $\Delta t_{bu}(\Delta T^*) \approx \Delta t_{pl}$ at a critical undercooling ΔT^*. One may observe GR microstructure, if $\Delta t_{bu} < \Delta t_{pl}$, in which break-up occurs before the sample has had time to completely solidify, and one may observe CG microstructure, if $\Delta t_{bu} > \Delta t_{pl}$. In Karma's model the problem of determining the critical undercoolings ΔT^* has been reduced to calculating the break-up time Δt_{bu}. From [7,8] one gets

$$\Delta t_{bu}(\Delta T) \approx \frac{3}{2}\frac{R_T^3(\Delta T)}{d_0}\frac{c_p k_e \Delta_e}{DQ}, \tag{8}$$

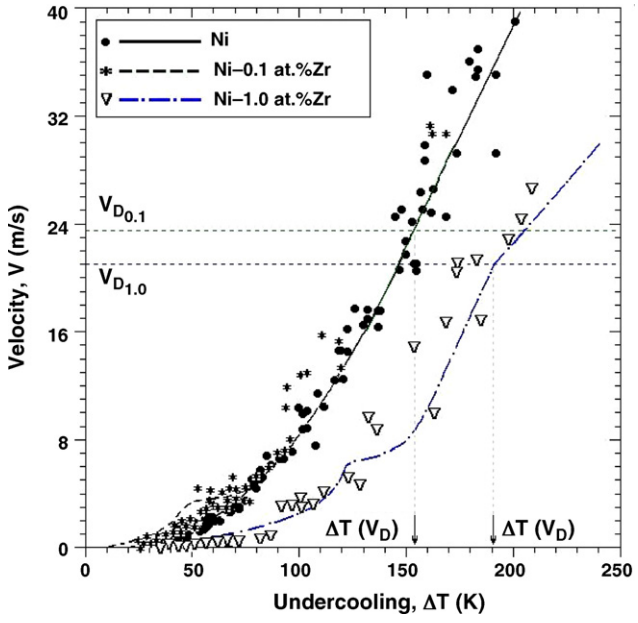

Fig. 3. Theoretical predictions "dendrite growth velocity vs. undercooling" in comparison with present experimental data. Notations $V_{D0.1}$ and $V_{D1.0}$ are the speed for solute diffusion in bulk liquid for the $Ni_{99.9}Zr_{0.1}$ alloy and the $Ni_{99}Zr_1$, respectively.

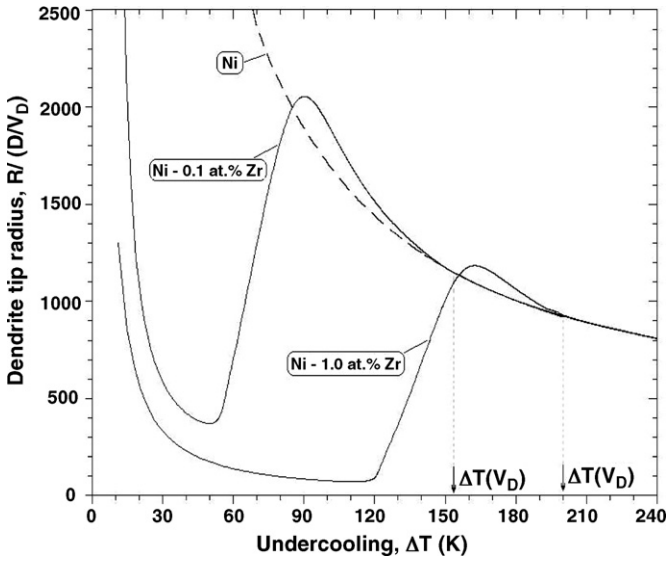

Fig. 4. Computed dendrite tip radius R vs. undercooling ΔT using Eqs. (1)–(7). The complete transition from the solutal and thermal dendrite growth to the thermal dendrite growth occurs with a break-point in curves at $\Delta T(V_D)$.

where R_T is the dendrite trunk radius and $\Delta_e = m_e C_0(k_e - 1)/k_e$ is the equilibrium solidification interval between liquidus and solidus in the phase diagram of the alloy. The trunk radius is correlated to the dendrite tip radius, $R(\Delta T)$, via a proportionality constant, $z = R_T(\Delta T)/R(\Delta T)$. This constant is determined by taking the ratio of the trunk radius, measured from micrographs of solidified samples, to the calculated tip radius at the same undercooling. This procedure yields an approximately constant value of $z \approx 20$ which was used in previous calculations [2,7]. Thus, comparing $\Delta t_{bu}(\Delta T)$ with Δt_{pl} one may predict the appearance of a certain type of microstructure (CG or GR).

The results of calculation of $\Delta t_{bu}(\Delta T)$ in comparison with experimental data for Δt_{pl} are shown in Fig. 2 (bottom). It can be seen that the results by Eq. (8), in principle, describe the critical undercoolings for transitions CG ↔ GR. A closer look to Fig. 2 (top) shows that there are two *regions* of undercooling, $37\,K < \Delta T < 80\,K$ and $123\,K < \Delta T < 130\,K$, for the transitions between CG and GR microstructures. The reason might be the forced melt flow in the levitated droplets. The dendrite tip radius R depends on convection in the melt and, as a consequence, the radius of the dendrite trunk R_T, too. A dendrite growth model with convective flow may lead to elimination of this uncertainty in comparison with experimental findings [12].

6. Conclusions

(i) New experimental data on solidification kinetics, crystal microstructure and fragmentation in undercooled Ni–Zr alloys have been obtained. Solidification and microstructure were investigated in droplets processed by electromagnetic levitation technique using capacity proximity sensor (CPS) and a high-speed camera (HSC) for dendrite growth velocity measurement.

(ii) Experimental evidence and modeling results show that small controlled amounts of Zr in Ni (on the level of 0.1 at.% Zr and smaller) give enhancement of the dendrite growth velocity in comparison with "nominally pure" nickel.

(iii) The complete sequence of solidified dendritic microstructure is given by CG ($\Delta T < 35\,K$) → GR ($80\,K < \Delta T < 123\,K$) → CG ($130\,K < \Delta T < 177\,K$) → GR ($\Delta T > 177\,K$). In the transition regions $37\,K < \Delta T < 80\,K$ and $123\,K < \Delta T < 130\,K$ both microstructures (CG and GR) may occur.

(iv) The local non-equilibrium model predicts the abrupt change of growth kinetics with the break point in both the "velocity V–undercooling ΔT" relationship and the "tip radius R–undercooling ΔT" relationship. This break point occurs at critical undercooling ΔT^* and solidification velocity $V = V_D$ for the onset of the diffusionless growth of crystals.

Acknowledgements

This work was supported by the German Research Foundation (DFG) under the project No. He 1601/13.

References

[1] C.B. Arnold, M. Aziz, M. Schwarz, D.M. Herlach, Phys. Rev. B 59 (1999) 334.
[2] M. Schwarz, Kornfeinung durch Fragmentierung von Dendriten, Ph.D. Thesis, Ruhr-Universität Bochum, 1998.
[3] D.M. Herlach, Annu. Rev. Mater. Sci. 21 (1991) 23.
[4] J. Lipton, W. Kurz, R. Trivedi, Acta Metall. 35 (1987) 957.
[5] W.J. Boettinger, S.R. Coriell, R. Trivedi, in: R. Mehrabian, P. Parrish (Eds.), Rapid Solidification Processing: Principles and Technologies IV, Claitor's, Baton Rouge, Louisiana, 1988, p. 13.
[6] M. Aziz, T. Kaplan, Acta Metall. 36 (1988) 2335.
[7] M. Schwarz, A. Karma, K. Eckler, D.M. Herlach, Phys. Rev. Lett. 73 (1994) 1380.
[8] A. Karma, Int. J. Non-Equilib. Process. 11 (1998) 201.
[9] P.K. Galenko, D.A. Danilov, Phys. Lett. A 235 (1997) 271; P.K. Galenko, D.A. Danilov, J. Cryst. Growth 197 (1999) 992.
[10] D.M. Herlach, R. Willnecker, F. Gillessen, in: Proceedings 5th European Symposium on Materials Science under Microgravity, ESA SP-2 22, ESA, Noordwijk, Netherlands, 1985, p. 399.
[11] K. Eckler, M. Kratz, I. Egry, Rev. Sci. Instrum. 64 (9) (1993) 2639.
[12] D.M. Herlach, P.K. Galenko, this issue.
[13] D.M. Herlach, O. Funke, G. Phanikumar, P. Galenko, in: M. Rappaz, C. Beckermann, R. Trivedi (Eds.), Solidification Processes and Microstructures, TMS, Warrendale, Pennsylvania, 2004, p. 277.
[14] P. Galenko, D. Herlach, G. Phanikumar, O. Funke, in: P. Vincenzini, A. Lami (Eds.), Computational Modeling and Simulation of Materials, Techna Group, Faenza, Italy, 2004, p. 565.
[15] K. Eckler, R.F. Cochrane, D.M. Herlach, B. Feuerbacher, M. Jurisch, Phys. Rev. B 45 (1992) 5019.
[16] P.K. Galenko, Preprint: Atomic exchange at the solid–liquid interface in rapid solidification of a binary system, 2003.
[17] P.K. Galenko, D.A. Danilov, Phys. Lett. A 272 (2000) 207.
[18] P. Galenko, Phys. Rev. B 65 (2002) 144103.
[19] P. Galenko, S. Sobolev, Phys. Rev. E 55 (1997) 343.
[20] E. Brener, D. Temkin, Preprint: Dendritic growth in supercooled binary melt at arbitrary Peclet numbers, 1996.
[21] H. Müller-Krumbhaar, T. Abel, E. Brener, M. Hartmann, N. Eissfeldt, D. Temkin, JSME Int. J. B 45 (1) (2002) 129.
[22] E. Brener, V.I. Melnikov, Adv. Phys. 40 (1991) 53.